EXPERIMENTAL INVESTIGATION AND COMPUTATIONAL FLUID DYNAMICS ANALYSIS OF A AIR COOLED CONDENSER HEAT PIPE

by

Arul Selvan ANNAMALAI [a*] ***and Velraj RAMALINGAM*** [b]

[a] Mechanical Engineering Department, Anna University, Chennai, Tamil Nadu,India
[b] Institute for Energy Studies, Anna University, Chennai, Tamil Nadu, India

Original scientific paper
UDC: 621.573/.574
DOI: 10.2298/TSCI100331023A

Heat pipe of one meter length and 0.031 m outer diameter was constructed and the experiments are conducted to determine the surface and vapour temperature at steady and transient conditions for two different input power in the evaporator section and cooling the condenser section by air. A computational fluid dynamics analysis was also carried and the results under steady-state conditions are compared with the results obtained from the experiments.

Key words: heat pipe, air cooled condenser, computational fluid dynamics analysis

Introduction

Heat pipe is an evaporation-condensation device for transferring heat in which the latent heat of vaporization is utilised to transport heat over long distances with a corresponding small temperature difference. The heat transport is realized by means of evaporating a liquid in the heat input region (called the evaporator) and subsequently condensing the vapor in a heat rejection region (called the condenser). Closed circulation of the working fluid is maintained by capillary action and/or bulk forces. Heat pipes are constructed usually using copper, nickel, stainless steel, molybdenum containers and the working fluids are usually water, cesium, sodium, lithium, bismuth, *etc*. The advantage of using a heat pipe over other conventional heat exchange methods is that large quantities of heat can be transported through a small cross-sectional area over a considerable distance with no additional power input to the system. Heat pipes have found applications in a wide variety of areas such as energy conversion system, cooling of nuclear and isotope reactor, cooling of electronic equipment, and high performance space application.

Some of the important studies carried out by the researchers on low temperature heat pipe are summarized in this section.

Faghri *et al*. [1] studied the effect of axial conduction in the fluid and the pipe wall of the heat pipe for forced convective laminar flow with blowing and suction at the impermeable wall. Faghri *et al*. [2] studied numerically the effect of conjugate heat transfer,

* Corresponding author; e-mail:velrajr@annauniv.edu

vapour compressibility and viscous dissipation for compressible and incompressible model. Chen *et al.* [3] studied both single and multiple heat sources in a 2-D axisymmetric cylindrical heat pipe. A coupled analysis of the wall, wick and vapour regions was conducted. Both sodium and water were considered as the working fluids. The solutions were compared against the experimental results for the vapour and wall temperature at high and low operating temperatures for the operating conditions considered. Compressibility effects were found to be very important. Faghri *et al.* [4] observed the overall performance of the concentric annular heat pipe with an emphasis on increase in the heat transport capacity as compared to the conventional heat pipe and also theoretically predicted the capillary limitation in a concentric annular heat pipe. Cao *et al.* [5] mathematically investigated the transient response of heat pipe to a pulsed heat input. Chang [6] developed the mathematical model to derive the effective thermal conductivity and porosity of the copper screened wick. The mathematical results were compared with the previous experimental results and expressions. Pruzan *et al.* [7] developed a model for predicting peak steady-state heat flux limit as a function of wick structure parameters and capillary pumping requirements. Faghri *et al.* [8] determined experimentally the capillary limit for single and multiple evaporator operating modes and also determined the temperature difference between the wall and the vapour on increasing the heat flux. Cao *et al.* [9] numerically analysed the transient and steady-state temperature distribution of leading edge heat pipe with uniform and non-uniform heat distribution. Cao *et al.* [10] numerically predicted the dynamics of the heat pipe from the frozen state to steady-state operation.

Schmalhofer *et al.* [11], determined the transient and steady-state temperature in the wall and the vapour region for step heat input of 50 W and 150 W, respectively, and also analytically predicted the capillary limit for circumferentially and block heated heat pipe. El-Genk *et al.* [12] investigated experimentally the vapour temperature and the effective power throughput as functions of the electric power input and the water mass flow rate in the cooling jacket of the condenser section. Tournier *et al*. [13] theoretically developed a heat pipe transient analysis model. The calculated transient and steady-state values were compared with the experimental results. Kim *et al*. [14] experimentally and analytically investigated the entrainment phenomenon in the capillary-driven heat pipe and also theoretically investigated the capillary limitation as a function of vapour temperature for three different mesh numbers. Harley *et al.* [15] numerically analysed the transient and steady-state temperature distribution in the wall and wick with pulsed heat input and studied the vapour dynamics of gas loaded heat pipe. Ma *et al.* [16] experimentally investigated the heat transport and maximum unit effective area heat transport in triangular grooves. Peterson *et al.* [17] mathematically predicted the maximum heat transport in micro heat pipes. Ma *et al.* [18] predicted the minimum meniscus radius and the maximum capillary heat transport limit in micro heat pipes. Thomas *et al.* [19] examined the steady-state performance of a helically grooved copper-ethanol heat pipe under various heat inputs and transverse body force field.

Hopkins *et al.* [20] experimentally investigated the steady-state performance characteristics of three individual copper-water flat miniature heat pipes for horizontal and vertical orientation. Wang *et al.* [21] experimentally investigated the thermal performance of a flat plate heat pipe. Zhu *et al.* [22] predicted the performance of a disk-shaped heat pipe and presented the optimum design obtained from the parametric study and the analysis of the boiling limitation. Zhu *et al.* [23] analysed the effects of liquid-vapour interfacial hydrodynamic coupling in the porous wick of the cylindrical heat pipe. The vapour and liquid velocity and pressure distribution are predicted. In addition the steady-state vapour and wall

temperature distribution through the heat pipe are also reported by them for a given heat input in the evaporator section and a convective boundary condition in the condenser section. Wang *et al.* [24] analytically predicts the transient performance of a flat plate heat pipe for startup and shutdown operations. Vadakkan *et al.* [25] analyzed the transient and steady-state performance of flat heat pipes under the action of discrete multiple heat sources. Williams *et al.* [26] determined the heat transfer limit of a step graded metal felt wick, explained experimentally and theoretically the cause of the failure and proposed the three hypotheses. The first one is that the ineffective sealing of the wick results in an exposed pore much greater in size than the measured effective radius, causing a premature capillary heat transfer limit failure. The second is that the liquid receding into the graded top layer of the wick results insignificant vapour flow through this layer causing an unaccounted vapour pressure drop and a premature capillary heat transfer limit failure. The third one is the nucleate boiling occurring within the wick resulting in a boiling heat transfer limit failure. Wang *et al.* [27] experimentally and analytically investigated the maximum heat transport capacity with the effects of mesh number, wire diameter, number of layers and tilt angle. Mahmood *et al.* [28] carried out an experimental investigation on the performance limitation of micro heat pipe of non-circular cross-section. They have analysed three different cross-sections (circular, semicircular, and rectangular) having same hydraulic diameter *(D* = 3 mm) with 3 different inclination angles (0°, 45°, 90°) using water as the working fluid. Mwaba *et al.* [29] studied numerically the influence of wicking structure on heat pipe performance. Han *et al.* [30] studied the thermal characteristics of grooved heat pipe with hybrid nanofluids and analysed for the parameters such as volume concentration, heat pipe inclination, and cooling water temperature.

In the present work, a water heat pipe is experimentally investigated for two different values of surface heat flux given in the evaporator section of the heat pipe and cooling of the condenser section by atmospheric air. The transient surface and vapour temperature distribution along the length of the heat pipe are studied in detail. A steady computational fluid dynamics (CFD) analysis was carried out for the configuration used in the experimental investigation and the results are validated.

Experimental set-up

An experimental set-up as shown in fig. 1 is constructed with the physical dimensions as given in tab. 1. The heat pipe is of one meter length and is divided in three main sections namely evaporator, adiabatic, and condenser sections of 400 mm, 200 mm, and 400 mm, respectively. The heat pipe is made up of copper material and the wrapped copper screen is used as the wick material. The wick consists of 16 holes per inches. The thickness of the single wick layer is 0.5 mm and the wire diameter is 0.31 mm. The wrapped copper screen wick is rolled in a mandrel up to four turns. The porosity of wick structure is 0.74 which is evaluated using:

$$\varepsilon = 1 - \frac{\pi SNd}{4} \tag{1}$$

where N is the mesh number, S – the crimping factor (S = 1.05) and d – the wire diameter. The mandrel is inserted into the inner diameter of copper pipe and then the mandrel is removed such that the wick is in high contact with the inner surface of the pipe surface because of the elongation property of the wick material. The physical dimensions of the heat pipe is given in tab. 1.

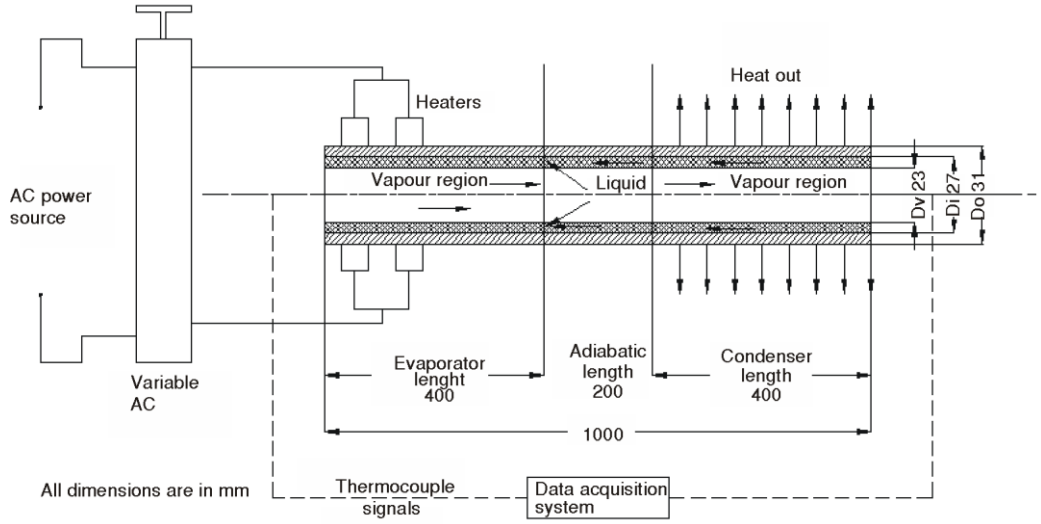

Figure 1. Schematic configuration of heat pipe with condenser section cooled convectively by atmospheric air

Table 1. Physical dimensions of heat pipe

Description	Dimension
Heat pipe total length	1000 mm
Evaporator section length	400 mm
Adiabatic section length	200 mm
Condenser section length	400 mm
Heat pipe inner diameter	27 mm
Heat pipe outer diameter	31 mm
Heat pipe wall thickness	2 mm
Mesh number of wick	16 holes per inch
Wick thickness	2 mm
Wick wire diameter	0.31 mm
Working fluid	Distilled water
No circumferential heater in the evaporator section	2
Insulating material	Glass wool

Stainless steel tube is drilled with very small holes at equal distances and ten numbers of copper-constantan thermocouple are inserted in the holes. This arrangement is inserted at the centre position of the copper tube. These thermocouples are used to measure the vapour temperature.

The end caps were welded in the copper tube. One end of the tube is connected to the vacuum pump and the other end is connected to the vessel containing distilled water. Control valves are also fixed at both ends and one vacuum gauge is mounted before the vacuum pump to measure the level of vacuum in the heat pipe. The heat pipe was evacuated to a pressure lower than atmospheric pressure and the distilled water from the vessel (250 ml) is sucked to the heat pipe using the vacuum available in the heat pipe.

The outer surface of the evaporator section consisted of a circumferential band heater. This heater assembly is powered by a variable AC transformer allowing the heat input to be varied. The power input is monitored by a voltmeter and an ampermeter connected to the variac. The surface temperature of the heat pipe is measured by ten copper constantan thermocouples equally spaced along the heat pipe. The evaporator and the adiabatic section of the heat pipe assembly are insulated with 3 inch glass wool insulation material. All the twenty

thermocouples used for the measurements are calibrated and found a maximum uncertainties of ±0.1°C. These thermocouples are connected to a data acquisition system (model Al8000+, AG make). The thermocouple locations are shown in fig. 2.

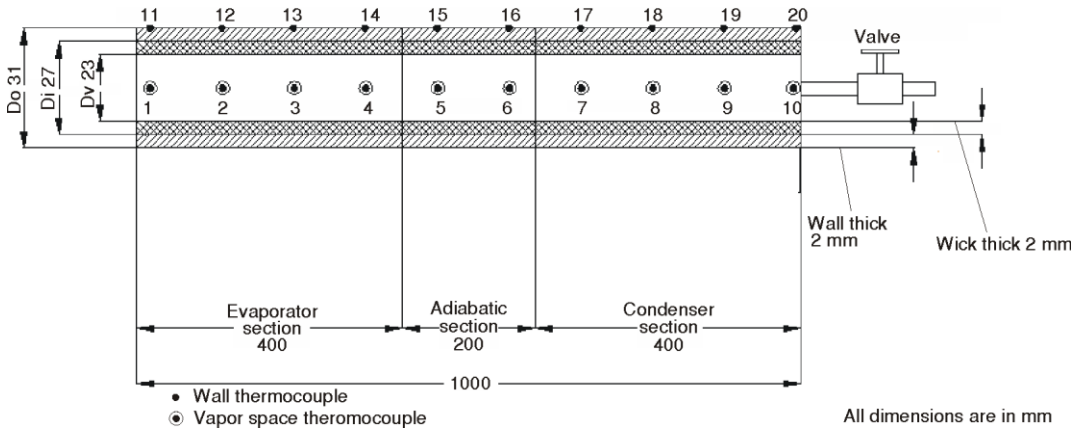

Figure 2. Heat pipe thermocouple locations

Several experimental runs are performed to find the temperature distribution of the vapour inside the heat pipe and also the surface temperature along the axial direction. In the evaporator section of 50 W power is supplied from the heat source, and the temperature variation at all the selected thermocouple locations are recorded continuously with respect to time. The observation are made until the condenser surface temperature attains steady-state. The experiments are repeated several times to confirm the repeatability of the results. The heater in the evaporator section is then set to 100 W and the same experiments are repeated several times.

Modeling and CFD analysis

The heat pipe configuration modeled for the present study is shown in fig. 3. The heat pipe consists of the evaporator section, transport section (adiabatic), and condenser section along the axial direction. There are three regions separated as vapour region, wick region and the wall region along the radial direction. The working fluid is assumed to be liquid phase in the wick region and vapour phase in the vapour region. When the evaporator is heated, the working fluid in the wick region

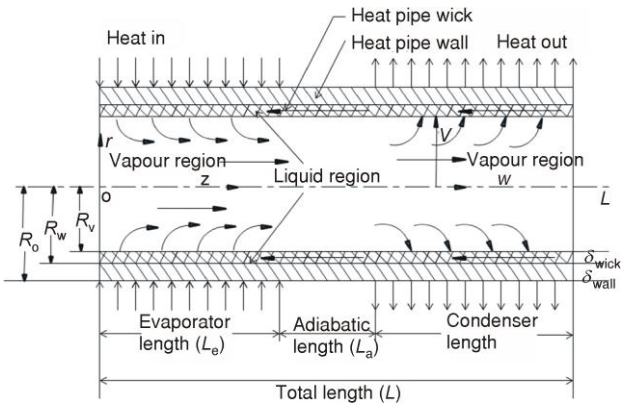

Figure 3. Physical model of the heat pipe

is vaporized to the vapour space and the vapor flows to the condenser region. In the condenser region, after the vapour releases its latent heat to the environment through the outer surface of the condenser, it returns to the wick region as saturated liquid.

The fundamental principles govern the flow and heat transfer in the heat pipe is expressed in terms of the following partial differential equations.

Vapour flow region

The governing equation for unsteady, compressible, laminar vapour flow with constant viscosity and viscous dissipation are given in eqs. (2)-(5).

Continuity equations:

$$\frac{\partial \rho_v}{\partial t} + \frac{1}{r}\frac{\partial}{\partial r}(\rho_v r V_v) + \frac{\partial}{\partial z}(\rho_v W_v) = 0 \tag{2}$$

Momentum equations:

– R-momentum

$$\rho_{\mathrm{v}}\left[\frac{\partial V_{\mathrm{v}}}{\partial t} + V_{\mathrm{v}}\frac{\partial V_{\mathrm{v}}}{\partial r} + W_{\mathrm{v}}\frac{\partial V_{\mathrm{v}}}{\partial z}\right] = -\frac{\partial p_{\mathrm{v}}}{\partial r} + \mu_{\mathrm{v}}\left[\frac{\partial^2 V_{\mathrm{v}}}{\partial z^2} + \frac{4}{3r}\frac{\partial}{\partial r}\left(r\frac{\partial V_{\mathrm{v}}}{\partial r}\right) + \frac{1}{3}\frac{\partial^2 W_{\mathrm{v}}}{\partial z \partial r} - \frac{4}{3}\frac{V_{\mathrm{v}}}{r^2}\right] \tag{3}$$

– Z-momentum

$$\begin{aligned}\rho_{\mathrm{v}}\left[\frac{\partial W_{\mathrm{v}}}{\partial t} + W_v\frac{\partial W_{\mathrm{v}}}{\partial z} + V_v\frac{\partial W_{\mathrm{v}}}{\partial r}\right] = \\ = -\frac{\partial p_{\mathrm{v}}}{\partial z} + \mu_{\mathrm{v}}\left\{\frac{4}{3}\frac{\partial^2 W_{\mathrm{v}}}{\partial z^2} + \frac{1}{r}\frac{\partial}{\partial r}\left(r\frac{\partial W_{\mathrm{v}}}{\partial r}\right) + \frac{1}{r}\frac{\partial}{\partial r}\left(r\frac{\partial V_{\mathrm{v}}}{\partial z}\right) - \frac{2}{3}\frac{\partial}{\partial z}\left[\frac{1}{r}\frac{\partial}{\partial r}(rV_{\mathrm{v}})\right]\right\}\end{aligned} \tag{4}$$

Energy equation:

$$\rho_{\mathrm{v}}C_{\mathrm{pv}}\left[\frac{\partial T_{\mathrm{v}}}{\partial t} + V_{\mathrm{v}}\frac{\partial T_{\mathrm{v}}}{\partial r} + W_{\mathrm{v}}\frac{\partial T_{\mathrm{v}}}{\partial z}\right] = k_{\mathrm{v}}\frac{1}{r}\frac{\partial}{\partial r}\left(r\frac{\partial T_{\mathrm{v}}}{\partial r}\right) + \frac{\partial^2 T_{\mathrm{v}}}{\partial z^2} + V_{\mathrm{v}}\frac{\partial p}{\partial r} + W_{\mathrm{v}}\frac{\partial p}{\partial z} + \mu_{\mathrm{v}}\phi$$

where

$$\phi = Z\left[\frac{\partial V_{\mathrm{v}}}{\partial r} + \left(\frac{V_{\mathrm{v}}}{r}\right)^2 + \left(\frac{\partial W_{\mathrm{v}}}{\partial z}\right)^2\right] + \left[\frac{\partial V_{\mathrm{v}}}{\partial z} + \left(\frac{\partial W_{\mathrm{v}}}{\partial r}\right)^2\right] - \frac{2}{3}\left[\frac{1}{r}\frac{\partial}{\partial r}(rV_{\mathrm{v}}) + \left(\frac{\partial W_{\mathrm{v}}}{\partial r}\right)^2\right] \tag{5}$$

Liquid flow region

The liquid flow in the wick is due to capillary action and is usually modeled as flow through porous medium. Liquid flow is considered as unsteady, incompressible laminar flow with negligible body forces. The governing equations are given in eqs. (6)-10).

$$\frac{1}{r}\frac{\partial}{\partial r}(rV_l) + \frac{\partial W_l}{\partial z} = 0 \tag{6}$$

Momentum equations:
– *R-momentum*

$$\frac{1}{\varepsilon}\frac{\partial V_l}{\partial t}+\frac{1}{\varepsilon^2}\left(V_l\frac{\partial V_l}{\partial r}+W_l\frac{\partial V_l}{\partial z}\right)=-\frac{1}{P_l}\frac{\partial P_l}{\partial r}-\frac{\mu_l V_l}{P_l k_l}+\frac{\mu_l}{P_l\varepsilon}\left[\frac{1}{r}\frac{\partial}{\partial r}\left(r\frac{\partial V_l}{\partial r}\right)-\frac{V_l}{r^2}+\frac{\partial^2 V_l}{\partial z^2}\right]_l \tag{7}$$

– *Z-momentum*

$$\frac{1}{\varepsilon}\frac{\partial W_l}{\partial t}+\frac{1}{\varepsilon^2}\left(V_l\frac{\partial W_l}{\partial r}+W_l\frac{\partial W_l}{\partial z}\right)=\frac{1}{P_l}\frac{\partial P_l}{\partial z}-\frac{\mu_l W_l}{P_l k_z}+\frac{\mu_l}{P_l\varepsilon}\left[\frac{1}{r}\frac{\partial}{\partial r}\left(r\frac{\partial W_l}{\partial r}\right)+\frac{\partial^2 W_l}{\partial z^2}\right] \tag{8}$$

Energy equation:

$$\rho_l C_{\mathrm{pl}}\frac{\partial T_l}{\partial t}+V_l\frac{\partial T_l}{\partial r}+W_l\frac{\partial T_l}{\partial z}=\frac{1}{r}\frac{\partial}{\partial r}\left(rk_{\mathrm{eff}}\frac{\partial T_l}{\partial r}\right)+\frac{\partial}{\partial z}\left(k_{\mathrm{eff}}\frac{\partial T_l}{\partial z}\right)$$

where

$$k_{\mathrm{eff}}=\frac{k_l\left[(k_l+k_{\mathrm{s}})-(1-\varepsilon)(k_l-k_{\mathrm{s}})\right]}{\left[(k_l+k_{\mathrm{s}})+(l-\varepsilon)(k_l-k_{\mathrm{s}})\right]} \tag{9}$$

Heat pipe wall region

The governing equation for the wall region is:

$$\rho_{\mathrm{w}} C_{\mathrm{pw}}\frac{\partial T_{\mathrm{w}}}{\partial t}=k_{\mathrm{w}}\left[\frac{l}{r}\frac{\partial}{\partial r}\left(r\frac{\partial T_{\mathrm{w}}}{\partial r}\right)+\frac{\partial^2 T_{\mathrm{w}}}{\partial z^2}\right] \tag{10}$$

The boundary conditions for evaporator, adiabatic, and condenser region at the various radii and also at the ends of the heat pipe are given in tab. 2.

The numerical solution to the governing equation of the fluid flow and heat transfer for the heat pipe is done using CFD software, to obtain the solution of the complete domain of interest. A commercial CFD package, ANSYS-CFX is used for the present simulations. The geometry of the computational domain is modeled in PRO E and the mesh preparation is done using CFX mesh in design modeler within ANSYS work bench. The isometric view of the meshed 3-D heat pipe is shown in fig. 4. The boundary in the outer pipe wall is divided into 3 regions. The evaporator region is provided with heat flux boundary condition while the condenser is subjected to convective boundary condition. The middle of heat pipe, adiabatic zone, is insulated and hence the heat flux boundary condition with a value of zero is given. Conduction exists between the wall and wick. Grid independence test was carried out and it was found that 14,000,000 unstructured tetrahedral cells were found to be suitable for the analysis with better accuracy. In the CFD

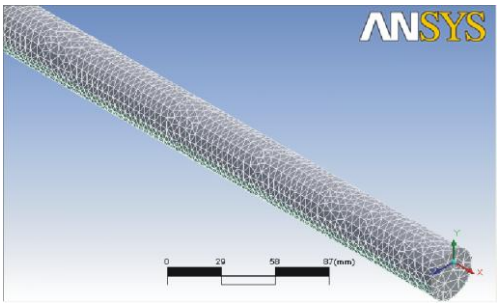

Figure 4. Isometric view of the meshed 3-D heat pipe

Table 2. Boundary condition

Radial/Axial locations	Evaporator $0 < Z < L_e$	Adiabatic $L_e < Z < L_e + L_a$	Condenser $L_e + L_a < Z < L$
Both ends of pipe ($Z = 0, L$)	$W = V = 0$ $\frac{\partial T}{\partial z} = 0$	– –	$W = V = 0$ $\frac{\partial T}{\partial z} = 0$
Centre line of the pipe ($r = 0$)	$\frac{\partial W_v}{\partial r} = 0$	$V_v = 0$	$\frac{\partial T_v}{\partial r} = 0$
Liquid vapour interface ($r = R_v$)	$T_s = \left[\frac{1}{T_0} - \frac{R}{h_{fg}} \ln \frac{P_s}{P_0}\right]^{-1}$ P_0 and T_0 reference saturation temperature and pressure $V_i = \frac{k_{eff} \frac{\partial T_l}{\partial r} - k_v \frac{\partial T_v}{\partial r}}{(h_{fg} + C_{pv} T_s) P_i}$ $W_i = 0$		
Wick – wall interface ($r = R_w$)	$k_w \frac{\partial T_w}{\partial r} = k_{eff} \frac{\partial T_l}{\partial r}$		
Outer pipe wall ($r = R_0$)	$q_e = -k_w \frac{\partial T_w}{\partial r}$	$\frac{\partial T_w}{\partial r} = 0$	$\frac{\partial T_w}{\partial r} = h(T_w - T_a)$

analysis, the surface convective heat transfer coefficient in the condenser side is given as 8.41 W/m^{2}K which is evaluated using the correlation:

$$\mathrm{Nu} = \left\{ 0.60 + 0.387 \left[\frac{\mathrm{Gr_D\ Pr}}{\left[1 + \left(\frac{0.559}{\mathrm{Pr}} \right)^{0.5625} \right]^{0.296}} \right]^{0.167} \right\}^2 \tag{11}$$

Results and discussion

Figure 5 shows the experimental result of the surface temperature distribution along the length of the heat pipe with power input in the evaporator section as 50 W at various time interval till the heat pipe attains steady-state. An axial distance of 0.2 m indicates the middle of the evaporator section. The axial distance between 0.4-0.6 m is the adiabatic zone and between 0.6-1.0 m is the condenser zone. It is seen from the figure that during the initial period of approximately 60 minutes, there is a continuous decrease in the temperature along the length of the heat pipe that shows the heat supplied in the evaporator section is utilised only to heat the water in the heat pipe. As time increases the process of evaporation and condensation process are clearly visible by the uniform surface temperature in the respective zones. The constant temperature of the surface in the evaporator zone is continued along its length up to adiabatic zone as there is no heat loss in this zone.

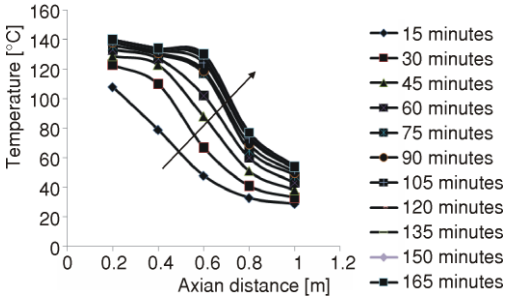

Figure 5. Surface temperature distribution along the axial direction of the heat pipe at various time intervals; *P* = 50 W

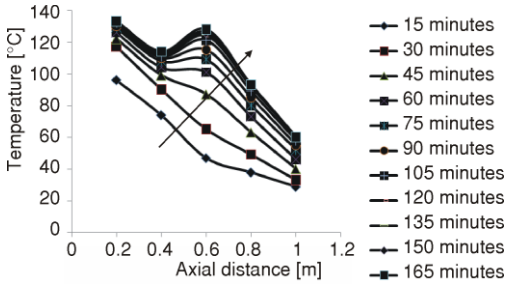

Figure 6. Vapour temperature distribution along the axial direction of the heat pipe at various time intervals; *P* = 50 W

Figure 6 shows the temperature distribution of the vapour along the length of the heat pipe. It is seen from the figure that there is a decrease in temperature along the length of evaporator and condenser zone at all times, while the temperature of the vapour in the adiabatic zone increases and the increasing magnitude is very high when the heat pipe attained the steady-state. In the evaporator zone heat is supplied by an electric coil and the coil surface area density is very high in the middle of the evaporator portion and hence the temperature of the vapour in the middle of the evaporator is high. In the adiabatic zone the vapour receives the heat from the wall of the heat pipe which it receives by axial conduction from the evaporator side of the heat pipe. Since the specific heat of the vapour is very low, the temperature of the vapour increases at a faster rate and when the system attains steady-state the vapour is in equilibrium with the surface temperature. In the condenser zone as the vapour rejects the heat to the atmosphere during the condensation, the vapour pressure decreases and hence further condensation occurs with reduced vapour pressure and its corresponding saturation temperature along the length of the condenser side also decreases. However the uniform surface temperature seen at the condenser section in fig. 5 indicates that there is a resistance for the heat dissipation to the surrounding due to the lower surface convective heat transfer coefficient.

Figure 7 shows the results of the average temperature distribution of the heat pipe with respect to time. When the heat pipe attained steady-state the evaporator surface reaches an average temperature of 136 °C and the condenser surface reaches an average temperature of 91 °C where the average vapour temperature in the evaporator and condenser are 123 °C and 93 °C, respectively.

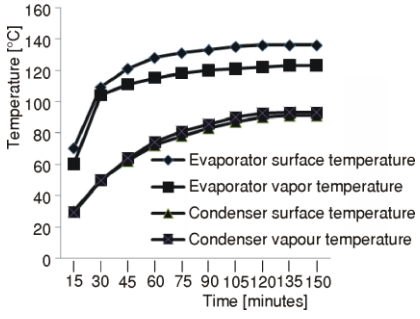

Figure 7. Experimental results of temperature distribution of the heat pipe *vs*. time; *P* = 50 W

Figure 8 shows the temperature variation of the vapour and the surface along the length of the heat pipe after it attained the steady-state. The temperature difference is very minimal or nearing zero at three locations (*i. e*. evaporator zone with highest heating intensity, end of the adiabatic zone and at the end of condenser zone). In an ideal heat pipe for the entire zone the temperature difference between the vapour and the surface should approach zero since evaporation and condensation are the processes with high heat transfer

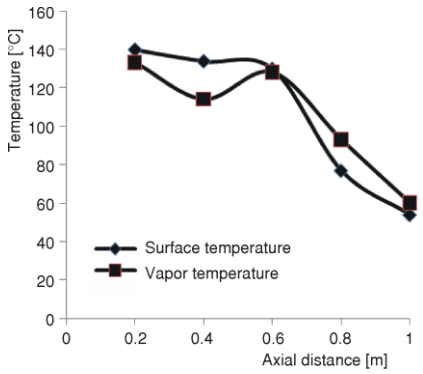

Figure 8. Temperature variation of the vapour and surface along the length of the heat pipe under steady-state condition; *P* = 50 W

coefficient. The increase in temperature difference in some region shows the reduction in the efficiency of operation. In the present case, the low surface convective heat transfer coefficient is the influencing resistance which affects the performance of the condensing process and sequentially the evaporation process in the heat pipe.

Figures 9-12 show the experimental results for a surface heat flux of 100 W in the evaporator section drawn similar to figs. 5-8 for a surface heat flux of 50 W. The surface temperature variation shown along the length of the heat pipe in fig. 9 follows the same pattern as explained for 50 W (fig. 5) except in the condenser region where there is a

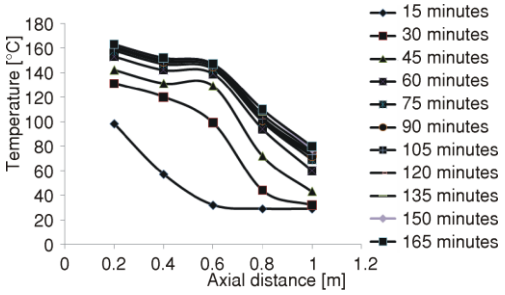

Figure 9. Surface temperature distribution along the axial direction of the heat pipe at various time intervals; *P* = 100 W

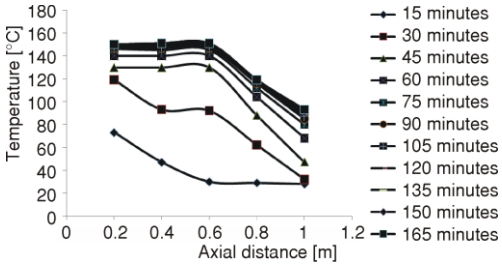

Figure 10. Vapour temperature distribution along the axial direction of the heat pipe at various time intervals; *P* = 100 W

comparatively higher decreases in temperature along the length of the condenser section. This is due to increase in temperature of the condenser surface at higher surface heat flux due to the lower outside surface convective heat transfer coefficient associated with the condenser section combined with the higher reduction in vapour pressure due to condensation of vapour along the length of the condenser section which is also seen from fig. 10. Further it is seen, from fig. 11, that at steady-state condition, the evaporator surface reaches an average temperature of 152 °C and the condenser surface reaches an average temperature of 117 °C where the average vapour temperature in the evaporator and condenser are 139 °C and 118 °C, respectively. The steady-state temperature variation of the vapour and the surface along the length of the evaporator is shown in fig. 12. An uniform temperature is seen in the surface and the vapour along the length of

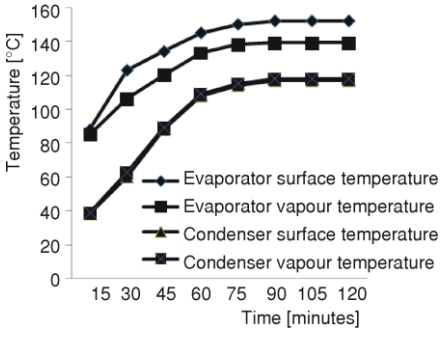

Figure 11. Experimental results of temperature distribution of the heat pipe *vs.* time; *P* = 100 W

the evaporator section and the difference in temperature between them is also very less unlike the decrease in temperature of the vapour seen at the end of evaporator section for the surface heat flux with 50 W. This shows that the size of the heat pipe is so large for 50 W and the evaporator section could handle higher heat flux if the condenser section is able to support for the same.

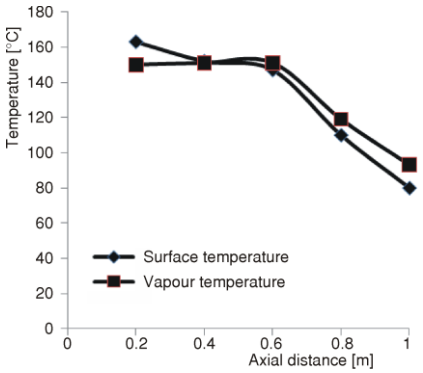

Figure 12. Temperature variation of the vapour and surface along the length of the heat pipe under steady-state condition; *P* = 100 W

The CFD analysis is restricted with the steady--state condition due to the non-availability of high performance computer which is required for the transient analysis with proper mesh size. The CFD analysis is performed for the configuration used in similar to the experimental investigation. The results obtained from the CFD analysis for the heat pipe with surface heat flux in the evaporator side as 50 W and 100 W are presented in figs. 13 and 14, respectively. Figure 13(a) shows the steady state vapour temperature distribution in the evaporator and condenser section of the heat pipe for the evaporator side surface heat flux of 50 W. Figures 13(b) and 13(c) show the steady-state surface temperature distribution within the evaporator and condenser section of the heat pipe respectively. Similar graphs are shown in figs. 14(a), 14(b), and 14(c) for the temperature distribution of the vapour in the evaporator and condenser section, surface temperature of the evaporator and surface temperature of the condenser respectively under steady state condition when input power in the evaporator section is 100 W. The above results are in good agreement with the results obtained from the experimental investigation. The

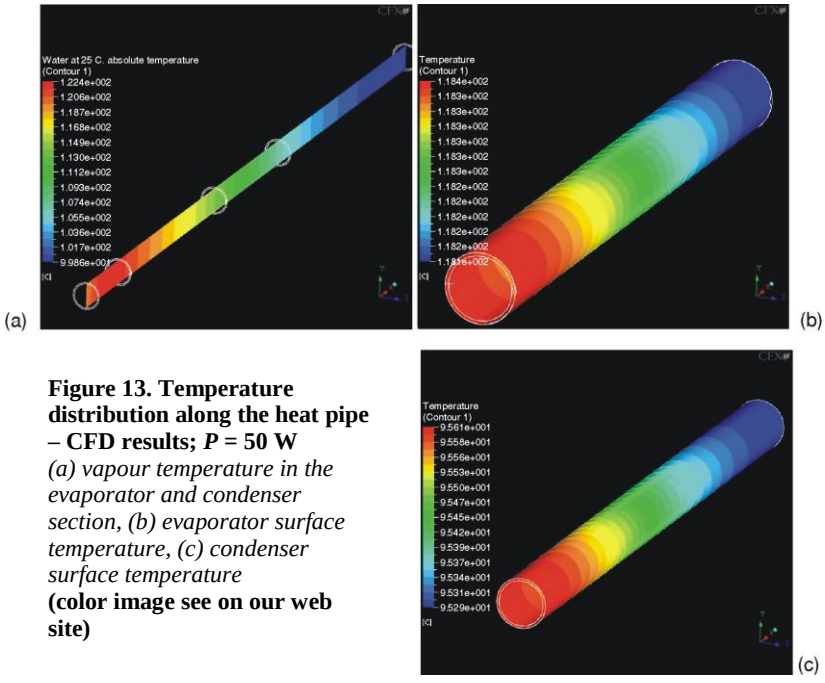

Figure 13. Temperature distribution along the heat pipe – CFD results; *P* = 50 W
(a) vapour temperature in the evaporator and condenser section, (b) evaporator surface temperature, (c) condenser surface temperature
(color image see on our web site)

average values of the vapour and the surface temperature obtained from the experimental and CFD analysis are presented in tab. 3 for comparison. It is observed from the table that as heat flux in the evaporator increases the system attains steady-state at higher temperature.

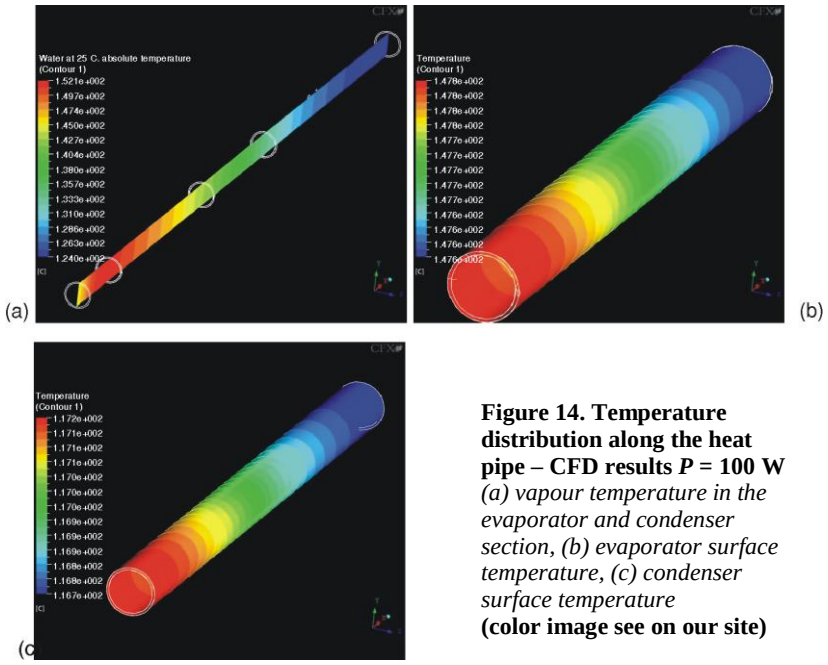

Figure 14. Temperature distribution along the heat pipe – CFD results *P* = 100 W
(a) vapour temperature in the evaporator and condenser section, (b) evaporator surface temperature, (c) condenser surface temperature
(color image see on our site)

Table 3. Comparison of steady-state temperature by CFD analysis and experimental investigation

Power input [W]	Section	Domain	CF CFD results [°C]	Experimental results [°C]
50	Evaporator	Surface	118	136
50	Evaporator	Vapour	118	123
50	Condenser	Vapour	99	93
50	Condenser	Surface	95	91
100	Evaporator	Surface	147	152
100	Evaporator	Vapour	145	139
100	Condenser	Vapour	124	118
100	Condenser	Surface	117	117

Conclusions

The experimental investigation and CFD analysis of a air cooled condenser heat pipe is carried out and the results are reported. The heat pipe attained near steady-state after 60 minutes of operation in both the cases of 50 W and 100 W heat flux provided in the evaporation section. The temperature variation along the length of heat pipe at various time intervals explaines clearly the process of evaporation and condensation that occurs inside the

heat pipe at varoius stages of operation. As surface heat flux in the evaporator increases the operating temperature of the heat pipe also increases which is due to the surface convective resistance of the condenser region. In the present case with air as the cooling medium in the condenser section, the low surface convective heat transfer coefficient is the influencing resistance which affects the performance of the condensing process and sequentially the evaporation process in the heat pipe. For efficient operation of the heat pipe, the condenser surface should be exposed with circulating water with high h value or higher heat transfer area is required with addition of fins in the condenser section.

Nomenclature

A – cross-sectional area, [m^2]
C_p – specific heat, [$Jkg^{-1}K^{-1}$]
d – diameter, [m]
Gr_D – Grashof number (= $g\beta\Delta TD^3/y^2$), [–]
h – heat transfer coefficient, [$Wm^{-2}K^{-1}$]
h_{fg} – latent heat, [Jkg^{-1}]
k – thermal conductivity, [$Wm^{-1}K^{-1}$]
l – length, [m]
$\dot{m}$ – mass flow rate, [kgs^{-1}]
Nu – Nusselt number (= hD/k), [–]
P – power, [W]
ΔP – pressure gradient, [Nm^{-2}]
Pr – Prandtl number (= $\mu C_p/k$), [–]
q – radial heat flux, [Wm^{-2}]
r – radial co-ordinate
T – local or mean temperature, [°C]
ΔT – temperature gradient, [°C]
t – thickness, [m]
v – radial velocity component, [ms^{-1}]
w – wick
w – axial velocity component, [ms^{-1}]
z – axial co-ordinate

Greek symbol

α – thermal diffusivity, [m^2s^{-1}]
β – coefficient of expansion, [K^{-1}]
δ – thickness, [m]
ε – wick porosity, [–]
μ – dynamic viscosity, [$kgm^{-1}s^{-1}$]
ν – kinematic viscosity, [m^2s^{-1}]
ρ – density, [kgm^{-3}]

Subscript

a – adiabatic
c – condenser
e – evaporator
eff – effective
in – inner
l – liquid
out – outer
v – vapour

References

[1] Faghri, A., Chen, M. M., Mahefkey, E. T., Simultaneous Axial Conduction in the Fluid and the Pipe Wall for Forced Convective Laminar Flow with Blowing and Suction at the Wall, *International Journal of Heat Mass Transfer, 32* (1989), 2, pp. 281-288
[2] Faghri, A., Chen, M. M., A Numerical Analysis of the Effects Conjugates Heat Transfer Vapor Compressibility and Viscous Dissipation in Heat Pipe, *Numerical Heat Transfer, Part A, 16* (1989), 3, pp. 389-405
[3] Chen, M. M., Faghri, A., An Analysis of the Vapor Flow and the Heat Conduction through the Liquid-Wick and Pipe Wall in a Heat Pipe with Single or Multiple Heat Sources, *International Journal of Heat Mass Transfer, 33* (1990), 9, pp. 1945-1955
[4] Faghri, A., Thomas, S., Performance Characteristics of a Concentric Annular Heat Pipe: 1 – Experimental Prediction and Analysis of the Capillary Limit, *Journal of Heat Transfer, 111* (1989), 4, pp. 844-850
[5] Cao, Y., Faghri, A., Transient Two-Dimensional Compressible Analysis for High-Temperature Heat Pipes with Pulsed Heat Input, *Numerical Heat Transfer, Part A, 18* (1990), 4, pp. 483-502
[6] Chang, W. S., Porosity and Effective Thermal Conductivity of Wire Screens, *Journal of Heat Transfer, 112* (1990), pp. 5-9
[7] Pruzan, D. A., *et al*., Design of High-Performance Sintered-Wick Heat Pipes, *International Journal of Heat Mass Transfer, 34* (1990), 6, pp. 1417-1426

[8] Faghri, A., Buchko, M., Experimental and Numerical Analysis of Low-Temperature Heat Pipes with Multiple Heat Sources, *Journal of Heat Transfer, 113* (1991), pp. 728-734
[9] Cao, A., Faghri, A., Transient Multidimensional Analysis of Nonconventional Heat Pipes with Uniform and Nonuniform Heat Distributions, *Journal of Heat Transfer, 113* (1991), pp. 995-1002
[10] Cao, Y., Faghri, A., A Numerical Analysis of High-Temperature Heat Pipe Startup from the Frozen State, *Journal of Heat Transfer, 115* (1993), pp. 247-251
[11] Schmalhofer, J., Faghri, A., A Study of Circumferentially – Heated and Block – Heated Heat Pipes – 1, Experimental Analysis and Generalized Analytical Prediction of Capillary Limits, *International Journal of Heat Mass Transfer, 36* (1993), 1, pp. 201-212
[12] El-Genk, M., Hung, L., An Experimental Investigation of the Transient Response of a Water Heat Pipe, *International Journal of Heat Mass Transfer, 36* (1993), 15, pp. 3823-3830
[13] Tournier, J. M., El-Genk, M. S., A Heat Pipe Transient Analysis Model, *International Journal of Heat Mass transfer, 37* (1994), 5, pp. 753-762
[14] Kim, B. H., Peterson, G. P., Analysis of the Critical Weber Number at the Onset of Liquid Entrainment in Capillary-Driven Heat Pipes, *International Journal of Heat Mass Transfer, 38* (1994), 8, pp. 1427-1442
[15] Harley, C., Faghri, A., Transient Two-Dimensional Gas Loaded Heat Pipe Analysis, *Journal of Heat Transfer, 116* (1994), 3, pp. 716-723
[16] Ma, H. B., Peterson, G. P., Experimental Investigation of the Maximum Heat Transport in Triangular Grooves, *Journal of Heat Transfer, 118* (1996), 8, pp. 740-746
[17] Peterson, G. P., Ma, H. B., Theoretical Analysis of the Maximum Heat Transport in Triangular Grooves: A Study of Idealized Micro Heat Pipes, *Journal of Heat Transfer, 118* (1996), 4, pp. 731-739
[18] Ma, H. B., Peterson, G. P., The Minimum Meniscus Radius and Capillary Heat Transport Limit in Micro Heat Pipes, *Journal of Heat Transfer, 120* (1998), 1, pp. 227-233
[19] Thomas, S. K., Klasing, K., Yerkes, K. L., The Effects of Transverse Acceleration – Induced Body Forces of the Capillary Limit of Helically Grooved Heat Pipes, *Journal of Heat Transfer, 120* (1998), pp. 441-451
[20] Hopkins, R., Faghri, A., Khrustalev, D., Flat Miniature Heat Pipes with Micro Capillary Grooves, *Journal of Heat Transfer, 121* (1999), 1, pp. 102-109
[21] Wang, Y., Vafai, K., An Experimental Investigation of the Thermal Performance of an Asymmetrical Flat Plate Heat Pipe, *International Journal of Heat Mass Transfer, 43* (2000), pp. 2657-2668
[22] Zhu, N., Vafai, K., Optimization of Asymmetrical Disk – Shaped Heat Pipes, *AIAA Journal of Thermophysics and Heat Transfer, 10* (1996), pp. 179-182
[23] Zhu, N., Vafai, K., Analysis of Cylindrical Heat Pipes Incorporating the Effects of Liquid – Vapor Coupling and Non-Darcian Transport – A Closed Form Solution, *International Journal of Heat and Mass Transfer, 42* (1999), pp. 3405-3418
[24] Wang, Y., Vafai, K., Transient Characterization of Flat Plate Heat Pipes During Startup and Shutdown Operations, *International Journal of Heat Mass Transfer, 43* (2000), pp. 2641-2655
[25] Vadakkan, U., Garimella, S. V., Murthy, J. Y., Transport in Flat Heat Pipes at High Heat Fluxes from Multiple Discrete Sources, *Journal of Heat Transfer, 126* (2004), pp. 347-354
[26] Williams, R. R., Harris, D. K., The Heat Transfer Limit of Step-Graded Metal Felt Heat Pipe Wicks, *International Journal of Heat Mass Transfer, 48* (2005), 2, pp. 293-305
[27] Wang, G. Y., Peterson, G. P., Investigation of a Novel Flat Heat Pipe, *Journal of Heat Transfer, 127* (2005), 2, pp. 165-170
[28] Mahmood, S. L., Akhanda, A. R., Experimental Study on the Performance Limitation of Micro Heat Pipes of Non Circular Cross – Sections, *Thermal Science, 12* (2008), 3, pp. 91-102
[29] Mwaba, M. G., Huang, X., Gu, J., Influence of Wick Characteristics on Heat Pipe Performance, *International Journal of Energy Research, 30* (2006), pp. 489-499
[30] Han, W. S., Rhi, S. H., Thermal Characteristics of Grooved Heat Pipe with Hybrid Nanofluids, *Thermal Science, 15* (2011), 1, pp. 195-206

Paper submitted: March 30, 2010
Paper revised: April 13, 2010
Paper accepted: March 16, 2010